JOURNAL OF GEOPHYSICAL RESEARCH, VOL. 105, NO. B1, PAGES 663–680, JANUARY 10, 2000

Active deformation in eastern Indonesia and the Philippines from GPS and seismicity data

Corné Kreemer and William E. Holt

Department of Geosciences, State University of New York at Stony Brook

Saskia Goes[1] and Rob Govers

Institute of Earth Sciences, Utrecht University, The Netherlands

Abstract. In this study we combine Global Positioning System (GPS) velocities with information on the style of regional seismicity to obtain a self-consistent model velocity and strain rate field for the entire eastern Indonesia and Philippines region. In the process of interpolating 93 previously published GPS velocities, the style and direction of the seismic strain rate field, inferred from earthquakes with $M_0 < 1 \times 10^{20}$ N m (from the Harvard centroid moment tensor catalog), are used as constraints on the style and direction of model strain rates within the plate boundary zones. The style and direction of the seismic strain rate field are found to be self-similar for earthquakes up to $M_0 = 1 \times 10^{20}$ N m (equivalent to $M_W < 7.3$). Our inversion result shows the following: The Java Trench, which lacks any significant (historic) seismicity, delineates the Australian plate (AU) - Sunda block (Sunda) plate boundary west of the island of Sumba. East of Sumba, convergence is distributed over the back arc and Banda Sea, and there is no subduction at the Timor Trough, suggesting that the northern boundary of the AU plate runs north of this part of the Banda arc through the Banda Sea. In New Guinea most motion is taken up as strike-slip deformation in the northern part of the island, delineating the Pacific plate (PA) - AU boundary. However, some trench-normal convergence is occurring at the New Guinea Trench, evidence that the strain is partitioned in order to accommodate oblique PA-AU motion. PA-AU motion is consistent with NUVEL-1A direction, but ~ 8 mm yr^{-1} slower than the NUVEL-1A estimate for PA-AU motion. The Sulawesi Trench and Molucca Sea delineate zones of high strain rates, consistent with high levels of active seismicity. The Sulawesi Trench may take up some of the AU-Sunda motion. Philippine Sea plate motion is in a direction slightly northward of the NUVEL-1A estimate and is partitioned in some strike-slip strain rates along the Philippine Fault and relatively larger trench-normal convergence along the Philippine Trench and on the Philippine mainland in the southern Philippines and along the Manila Trench in the northern Philippine islands. The high level of strain rate along the Manila Trench is not released by any significant (historic) seismic activity. For the entire eastern Indonesia – Philippines region, seismicity since 1963 has taken up ~40% of the total moment rate inferred from our model.

1. Introduction

The eastern Indonesia and Philippines region is a complicated configuration of active plate boundaries that are readjusting in response to the collision of the Australian continent with the Sunda block. Global plate motion models describing the motion of the surrounding plates (e.g., NUVEL-1A [*DeMets et al.*, 1994]) do not define how strain rates are distributed in this diffuse zone of deformation. However, the recent availability of Global Positioning System (GPS) observations in this region provides an opportunity to address the following questions: (1) Which tectonic features delineate plate boundaries, and what is the distribution of the velocity gradient tensor field within the plate boundary zones that accommodates far-field plate motion? and (2) How does seismic strain rate release within these boundary zones compare with long-term total strain rates, inferred from GPS observations? By long-term strain rates we mean the strain rate field that accommodates plate motions over timescales that are less than the period over which plate motions change but a time period greater than several seismic cycles. This long-term strain rate field may therefore contain both an aseismic component and a seismic component, which we refer to as the long-term seismic strain rate field.

Both seismicity and geodetic data provide different types of information that allow one to estimate the long-term strain rate field within plate boundary zones. Accurate focal mechanisms from earthquakes are available since the establishment of the World-Wide Standardized Seismograph Network (WWSSN) in about 1964 and are only routinely available since the start of the Harvard centroid moment tensor (CMT) catalog (1977 to the present). This record spans only a small portion of the recurrence time of large events (which is

[1]Now at Institut für Geophysik, Eidgenossische Technische Hochschule Hönggerberg, Zurich.

Paper number 1999JB900356.
0148-0227/00/1999JB900356$09.00

100-200 years along major plate boundaries but could be thousands of years in areas away from major boundaries), which results in an incomplete sampling of the seismic cycle of larger events and may therefore not reflect average long-term (seismic) deformation. Nevertheless, seismicity provides important information on the geometry of seismic zones and on the style and localization of permanent deformation, and seismicity has been used to infer tectonics of the different (sub) regions [e.g., *McCaffrey*, 1988, 1989; *Cardwell and Isacks*, 1978; *Puspito and Shimazaki*, 1995]. However, seismic moments account for only 20% of the convergence near Timor [*McCaffrey*, 1988] and 5-20% in the highlands of New Guinea [*Abers and McCaffrey*, 1988]. This could suggest the presence of a large amount of aseismic deformation, but could also, owing to the shortness of the catalog, reflect an accumulating seismic deficit that may be recovered in large future events.

Geodetic measurements record complete deformation (seismic and aseismic) and therefore provide the best source for the direct estimate of the long-term total strain rate tensor field. However, geodetic data also have shortcomings such as the unknown contributions to the signal produced by coseismic and postseismic deformation, which can lead to misinterpretation of geodetic results. That is, motions may (partially) reflect transients associated with seismic deformation (however, when treated with care, these "artifacts" can be modeled quite accurately and removed from the signal [e.g., *Pollitz and Dixon*, 1998]). Motions measured using GPS may also indicate elastic deformation instead of permanent deformation. Earthquakes, on the contrary, are always indications of permanent deformation. Elastic deformation is more likely to be distinguished from permanent deformation with the use of a very dense GPS network. Such a dense network is capable of a relatively precise determination of the velocity gradient tensor field. However, dense distributions of GPS data are not available for many regions at present, which can result in problems of poor spatial resolution in the model estimate of the strain rate tensor field. A particular shortcoming associated with the measurement of elastic deformation is that the elastic strain rate field is generally smeared-out in comparison with the long-term strain rate field [*Shen-Tu et al.*, 1999]. However, GPS observations made over length scales several times the locking depth of major faults or length scales spanning entire plate boundary zones, often reflect full plate motion [e.g., *Gordon and Stein*, 1992; *Stein*, 1993], which is inferred from a 3 Ma average of seafloor spreading rates and transform fault trends [*DeMets et al.*, 1994].

In this paper we estimate model long-term strain rate fields using both GPS velocities and seismicity data. GPS data provide most of the information in our solutions on the velocity gradient tensor field, while mechanisms of small and moderate-sized earthquakes are used to help constrain the direction and style of strain in localized zones. The largest events also provide information on the type of faulting, but because of the brevity of the catalog, the strain tensor style inferred from the mechanisms of the largest events does not provide a statistically reliable estimate of the long-term, seismic strain tensor field. Both the magnitude and style of the long-term, seismic strain tensor field can only be inferred by observing several seismic cycles for the largest events. We assume that the portion of the catalog that can be determined to be self-similar can provide information on the long-term style of the seismic strain tensor field (but not magnitude). We therefore conduct a test to determine the magnitude range over which the events in the Harvard CMT catalog are self-similar.

The strength of our analysis is that we are able to combine GPS observations from many different studies with earthquake moment tensor information to infer one self-consistent kinematic model for the entire region. We compare our predicted total strain rate field with seismic moment release from earthquakes with $M > 7$ since 1963. Furthermore, we compare our predicted velocity field for the stable surrounding plates with NUVEL-1A plate motion estimates [*DeMets et al.*, 1994].

2. Regional Tectonic Setting

In the southeast Asian region, four main plates meet: the Sunda block (Sunda) and the Australian plate (AU), Philippine Sea plate (PH), and Pacific plate (PA) (or Caroline plate) (Figure 1). It is established that Sunda is an independent entity from the Eurasian plate with a distinct motion [e.g., *Cardwell and Isacks*, 1978; *Johnston and Bowin*, 1981; *Simons et al.*, 1999]. On the contrary, less clear evidence exists for the suggested presence of an independent Caroline plate south of the PH plate [*Weissel and Anderson*, 1978]. For the moment this region is assumed to be part of the Pacific plate, but we also investigate the possibility that an independent Caroline plate exists. Figure 1 shows the major tectonic features in this region.

The formation of the Indonesian island arc (i.e., the Sunda-Banda arc) is a direct consequence of the northward motion of the AU plate relative to Sunda. At present, this involves subduction of ~148 Ma old oceanic lithosphere [*Hamilton*, 1979] at the Java Trench, west of the island of Sumba. East of Sumba, collision between Australian continental lithosphere and the Banda arc (i.e., along the Timor Trough) and New Guinea has been ongoing since the late Miocene [*Dow and Sukamto*, 1984]. This setting provides the opportunity to study both the process of active arc-continent collision as well as the consequence of a lateral change from subduction to collision along the arc. The Flores and Wetar back arc thrusts are seismically much more active than the subduction thrust faults near the Timor Trough [*McCaffrey*, 1988]. This suggests a jump in the locus of convergence from the Java Trench to the back-arc east of 118°E, which has been recognized by others [e.g., *Audley-Charles*, 1975; *McCaffrey*, 1988]. Since 1903 only one large thrust event has occurred at the Java Trench (June 2, 1994, $M_w = 7.8$) (*Pacheco and Sykes* [1992] and Harvard CMT catalog).

In New Guinea, where the Australian and Pacific plates interact, three distinctive tectonic zones can be found: a young and strongly elevated fold-and-thrust belt (i.e., New Guinea Thrust Belt), a zone of major left-lateral strike-slip faults (with the Sorong and Tarera-Aiduna Faults being the most prominent [e.g., *Hamilton*, 1979]), and the New Guinea Trench (NGT) at which Pacific lithosphere is currently subducting. New Guinea accommodates highly oblique convergence between the PA and AU plates at an angle of ~60°, and earthquakes form a distributed zone of deformation in which strain partitioning has been recognized, involving both shortening and left-lateral shear [*Abers and McCaffrey*, 1988; *McCaffrey*, 1996].

Another zone of strain partitioning is recognized in the Philippines [*Fitch*, 1972] where the oblique convergence between PH and Sunda is partitioned in near-trench-normal

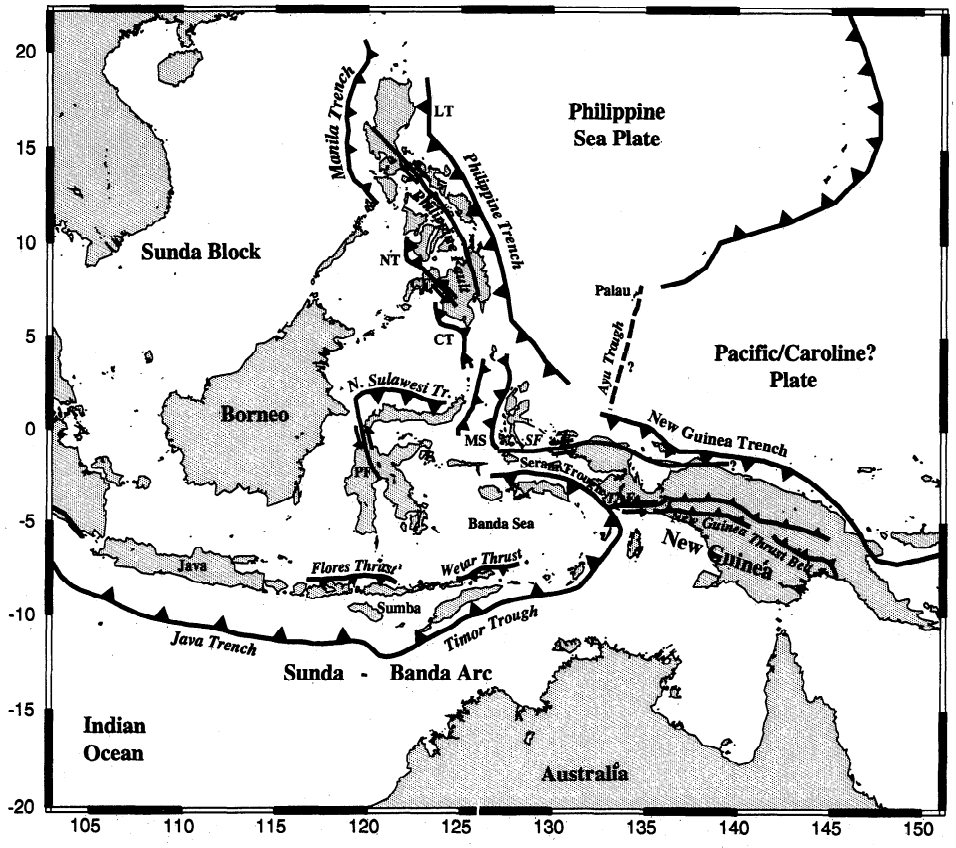

Figure 1. Tectonic map of eastern Indonesia and the Philippines (modified from *Hamilton* [1979]): LT, East Luzon Trough; CT, Cotabato Trench; CF, Cotabato Fault; NT, Negros Trench; MS, Molucca Sea; SF, Sorong Fault; TAF, Tarera-Aiduna Fault; PF, Palu Fault.

subduction at the Philippine Trench and left-lateral shear at the Philippine Fault [*Barrier et al.*, 1991]. However, recent GPS studies [e.g., *Rangin et al.*, 1997] show that in the northern Philippines most convergence is taken up at the Manila Trench, which yields low seismic activity and is of opposite polarity from the subduction process along the Philippine Trench. In the interior parts of the entire southeast Asian deformation zone there are regions such as the Molucca Sea (MS) collision zone and North Sulawesi Trench (NST) that both undergo high seismic activity associated with subduction. Although these regions have been studied in detail by *Silver et al.* [1983] and *McCaffrey*, [1982], respectively, their role in the large-scale accommodation of plate motions in the southeast Asia region has not been established.

3. Estimating a Self-Consistent Velocity and Strain Rate Field

We use the method of *Haines and Holt* [1993] to map seismic strain rate tensors and/or geodetic velocities into a complete, horizontal velocity gradient tensor field within the deformation zone. The complete, horizontal velocity gradient tensor field can be obtained when the strain rate field is known everywhere [*Haines*, 1982]. The three components of the strain rate tensor associated with horizontal deformation on the surface of the Earth $(\dot{\varepsilon}_{\theta\theta}, \dot{\varepsilon}_{\phi\phi}, \dot{\varepsilon}_{\theta\phi})$ determine a rotation vector function $\mathbf{W}(\hat{x})$, which describes the velocity field $\mathbf{u}(\hat{x})$,

$$\mathbf{u}(\hat{x}) = r\mathbf{W}(\hat{x}) \times \hat{x} \qquad (1)$$

where $\hat{x}$ is the unit radial position vector on the Earth's surface and r is the radius of the Earth. The rotation vector function $\mathbf{W}(\hat{x})$ is expressed using bicubic Bessel interpolation on a curvilinear grid [*De Boor*, 1978; *Haines et al.*, 1998]. The distribution of $\mathbf{W}(\hat{x})$ is determined through least squares minimization between observed and predicted strain rates within the grid areas shown in Figure 2. This procedure is extensively explained and used in other papers [e.g., *Holt and Haines*, 1995; *Tinnon et al.*, 1995; *Haines et al.*, 1998]. Figure 2 outlines the grid areas that are assumed rigid (Sunda, AU, and PH) as well the grid boundary within the Pacific plate that is also assumed rigid.

To obtain a model fit to the seismic strain rates, we perform the bicubic Bessel interpolation of the observed seismic strain rate values. The three horizontal components of strain rate uniquely define the horizontal velocity field $\mathbf{u}(\hat{x})$ [*Haines*, 1982; *Haines and Holt*, 1993]. To determine self-consistent strain rate fields associated with GPS observations, we use the same bicubic Bessel interpolation approach, but instead of matching strain rates to determine a continuous velocity field, GPS observations are matched subject to the constraint of minimal strain magnitude. A strain rate field is defined as self-consistent when it is associated with a velocity field and, as such, satisfies Saint Venant's compatibility relationships [e.g., *Love*, 1944; *Fung*, 1965]. In the procedure in which GPS velocities are matched by a model horizontal velocity field $\mathbf{u}(\hat{x})$, isotropic strain rate variances are assigned, a priori, to the strain rate tensor elements within areas. Higher variances are assigned to the plate boundary zones whose locations are

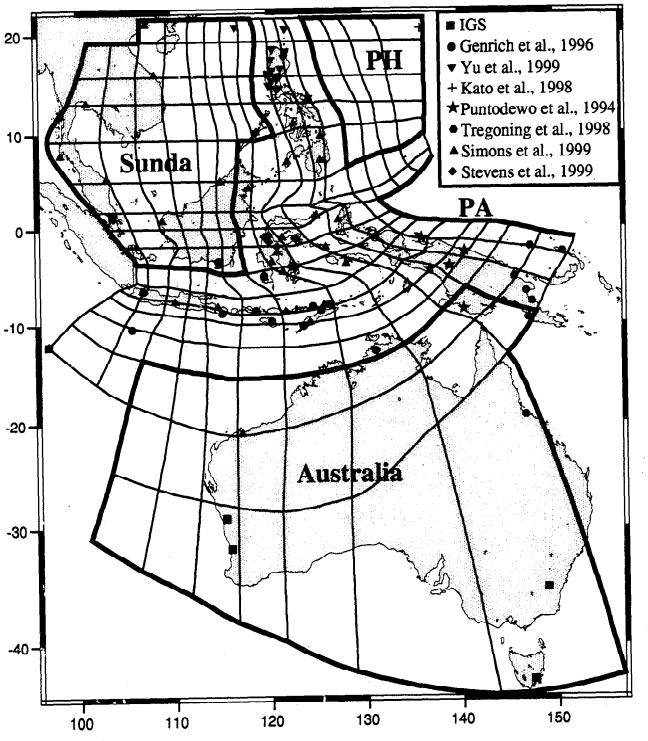

Figure 2. Grid used in the inversion. Bold solid lines connect or outline grid points that are considered part of rigid plates. These grid points specify four plate boundaries corresponding to the Sunda block and the Pacific plate (PA), Philippine Sea plate (PH), and Australian plate. All areas in between rigid zones are allowed to deform. Also shown are the locations and references of the Global Positioning System (GPS) velocities used in this study. IGS, International GPS Service.

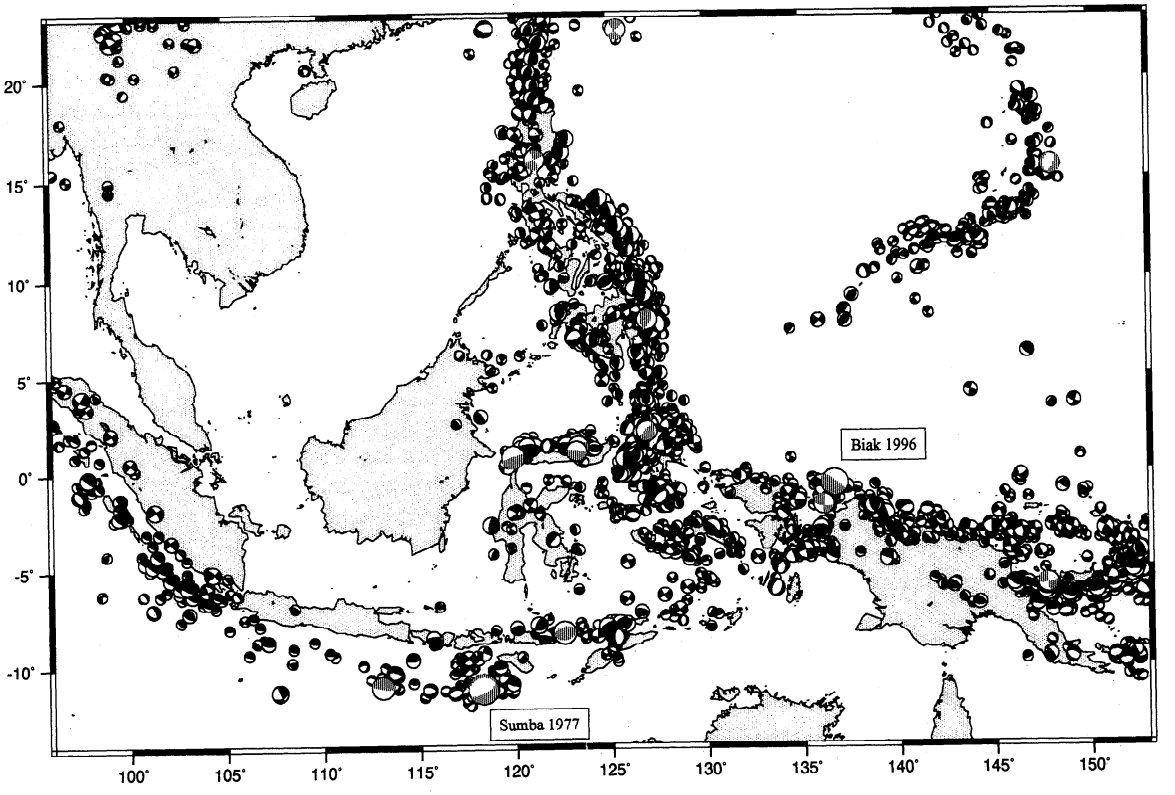

Figure 3. Focal mechanisms from the Harvard centroid moment tensor (CMT) catalog (January 1, 1977, to May 31, 1998. Mechanisms with solid and shaded fill are for earthquakes with $M_0 < 1 \times 10^{20}$ N m and $M_0 > 1 \times 10^{20}$ N m, respectively.

derived from the distribution of seismicity. Areas with higher assigned variances have the propensity to strain at higher rates in the fitting of GPS velocities. The isotropic variances allow the plate boundary zones to strain in any direction necessary to match GPS velocities.

Covariances can be made anisotropic such that the model strain rate field will match as closely as possible the expected directions of principal strain, inferred (in this case) from earthquake strain rates. Likewise, the covariances can also be constructed such that the model strain rate field matches the style of strain (dip-slip, strike-slip, or mixed) inferred from seismic strain rates (for more details, see *Haines et al.* [1998]). A confidence level of ±10° is placed on the directions of principal strain, but if earthquake activity is low or absent, covariances are made isotropic. It is important to note that only the direction and relative magnitude of the principal axes of strain rate are constrained a priori. We do not specify a priori the sign of strain. That is, the GPS data define whether the strain rates involve convergence or extension, or left, or right lateral shear.

4. Seismicity Data

To obtain an estimate of the seismic strain rate and velocity field, we use focal mechanism solutions from the Harvard centroid moment tensor (CMT) catalog [e.g., *Dziewonski et al.*, 1981, 1996, and references therein] (Figure 3). This catalog contains solutions for approximately all events with magnitude $M_w > 5.5$ within a time period of more than 21 years (January 1977 to May 1998). Only events with a depth less than 40 km are used, because we are solely interested in lithospheric deformation related to horizontal surface motions. Almost half of the moment in the catalog comes from only two events (Figure 4). These are the 1977 Sumba event ($M_w = 8.3$) and the 1996 Biak event in Irian Jaya ($M_w = 8.2$) (Figure 3). The Biak event is a shallow thrust event along the NGT. The Sumba event, located at the easternmost end of the Java Trench, has a normal fault mechanism ascribed to either breaking or bending of the downgoing slab [*Stewart*, 1978; *Spence*, 1986; *Lynnes and Lay*, 1988] and thus does not reflect horizontal plate motions.

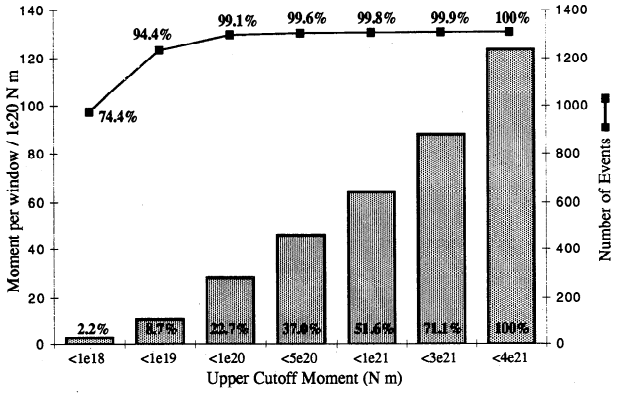

Figure 4. Distribution of number of events and seismic moment of the different magnitude windows for events shown in Figure 3. Percentages are relative to the total moment and relative to the total number of events in the entire CMT catalog for the region. Read 1e20 as 1×10^{20}.

4.1. Summing Earthquake Moment Tensors

A recent study in California [*Amelung and King*, 1997] showed that when averaged over a regional scale, strain released by small earthquakes follows closely the regional pattern of tectonic deformation. This holds for all but the largest events, indicating self-similarity over a broad range of magnitudes. The lack of self-similarity observed for the largest earthquakes [*Amelung and King*, 1997] is associated with a time interval that is too short to sample a complete set of events for that magnitude, rather than indicating inconsistency between the mechanisms of small and large events on the same fault. Hence a test of the self-similarity of the catalog is an important step necessary when one tries to infer patterns of the long-term strain rate field from a catalog that is too short to contain a complete sampling of the total magnitude range.

In order to perform a test of self-similarity of moment tensors in the catalog, first we split the total catalog (Figure 3) into seven magnitude windows with increasing upper moment cutoffs (Figure 4). The smallest window contains all moments less than 1×10^{18} N m, and the largest window covers the complete catalog. Figure 4 shows that 99% of the events in the catalog have a moment of $M_0 < 1 \times 10^{20}$ N m but contain less than a quarter of the total moment. Next we sum earthquake moment tensors for each of the seven different magnitude windows to infer a seismic strain rate tensor $\dot{\bar{\varepsilon}}_{ij}$ within the individual cells in the grid shown in Figure 2. The moment tensor summation follows from *Kostrov* [1974]:

$$\dot{\bar{\varepsilon}}_{ij} = \frac{1}{2\mu VT} \sum M_o m_{ij}, \tag{2}$$

where μ is the shear modulus, V is the cell volume (the grid area times the seismogenic thickness), T is the time period of the earthquake record, M_0 is the seismic moment, and m_{ij} is the unit moment tensor. We use a shear modulus of 3.5×10^{10} N m^{-2} and a 30 km thickness of the seismogenic zone. These parameters will only have an effect on the magnitude of deformation not on the style. The chosen value of these parameters does not affect our model with combined GPS and seismicity information, because then we use only the information about the style and direction of the inferred seismic strain rate field not the magnitude. The magnitude of total strain rate field is provided by geodetic measurements. In section 5 we first discuss the strain rate field based purely on seismicity.

4.2. Uncertainty Estimates in Seismic Strain Rates

There are two main sources of uncertainty when one tries to estimate the pattern of the long-term strain rate field from earthquake moment tensors. One source is due to the uncertainty in the seismic moment and fault plane solution, but a much more significant source of uncertainty is related to the distribution of earthquakes in space and time. This uncertainty is due to the fact that an earthquake catalog of short duration is a random sample from the long-term pattern of seismicity. This will influence any estimate of the long-term strain rate field [e.g., *Haines et al.*, 1998]. When we use only the Harvard CMT catalog, errors in focal mechanisms are expected to be small in comparison to errors that arise in the estimate of the long-term strain rate field, given the short duration of the catalog. Therefore it is sufficient to incorporate

only the uncertainty due to the short period of the catalog. We quantify this uncertainty by assuming that seismicity follows a Poisson probability distribution in which the moment tensor $M_o m_{ij}$ of each earthquake effectively makes a contribution of $\pm M_o m_{ij}$ to the uncertainties in the strain rates [*Shen-Tu et al.*, 1998]:

$$\mathrm{var}(\dot{\bar{\varepsilon}}_{ij}) = \sum \left(\frac{M_o m_{ij}}{2\mu VT} \right)^2. \quad (3)$$

The consequence of this definition of the variance is that the occurrence of a large number of earthquakes with fairly equal moment tensors in a certain (grid) area will lead to small standard errors in the strain rate relative to the total magnitude of seismic strain rate for that area. However, the addition of one significantly larger event for that area will dramatically increase the size of the standard error. This measure of uncertainty will be used when we test for the reliability of self-similarity in the catalog.

5. Results of the Self-Similarity Test

We determine a self-consistent seismic strain rate and velocity field, inferred from moment tensors within the four lowest magnitude windows. The three windows with $M_0 > 5 \times 10^{20}$ N m are dominated by a few large events (Figure 4), which produce a solution that yields high uncertainties in the estimate of a long-term seismic strain rate field (see equation (3)) and that exhibits grid areas with high strain rates next to regions with relatively little deformation. For all windows the observed seismic strain rates are smoothed over an area with a radius equivalent to one grid box in dimension [*Haines et al.*, 1998]. To quantify the self-similarity from one window to another we calculate for each of the four lowest magnitude windows the predicted average velocity for seven to eight points along both the New Guinea and southern Philippines Trenches. Given the uncertainty of the average velocity along these trenches a predicted azimuthal range is calculated. We choose these margins, because of the high seismic activity at the New Guinea and Philippine plate boundary zones, which makes a sensitivity test of the possible change of seismic deformation from one window to another viable. On the other hand, seismic strain rates for these windows are too small for the Sunda-Banda arc and NST to provide a meaningful quantification.

For the PA-AU motion, measured along the NGT, there is a clear self-similarity for the lower three windows (Figure 5). The azimuthal range is only a few degrees and increases only slightly over these magnitude windows (see Figure 6b for the complete velocity field associated with the largest of these three windows). It is noteworthy that the estimate is close in direction to PA-AU or Caroline-AU motions. For the window with $M_0 < 5 \times 10^{20}$ N m, azimuthal variations of velocity direction along the PA-AU margin are larger and no longer overlap with expected plate motion direction. For the predicted PH-AU motion, measured along the southern Philippines Trench, self-similarity clearly exists for the lowest two windows but not for the larger ones (Figure 5). However, predicted azimuths in the window with $M_0 < 1 \times 10^{20}$ N m approximate PH-AU NUVEL-1A direction.

On the basis of these results, we argue that the strain rate field from earthquakes up to $M_0 < 1 \times 10^{20}$ N m, which corresponds to $M_w < 7.3$, is self-similar along the Philippines-Sunda and New Guinea-Pacific system. That is, the catalog is self-similar over 2 orders of magnitude, which includes all but the largest 12 events. A close examination of the slip vectors of the 12 largest events ($M_w > 7.3$) indicates that they do not differ significantly in style from the much larger population of smaller events (see Figure 3) (an exception is the Sumba event, which has an anomalous style that has been discussed in section 4). However, we argue that self-similarity breaks down for these large magnitudes because the direction and style of the long-term strain rate tensor field that can be deduced from the few large events are not statistically reliable (equation (3)). On the other hand, the population of similarly sized events for $M_0 < 1 \times 10^{20}$ N m is large enough to provide a strain rate field that is statistically viable. Thus the lowest three magnitude windows can be used to define the expected style of the long-term seismic strain rate field (but not the magnitude). This conclusion is based on an average for the total region. We emphasize that when looking at a large region with a wide variety of tectonic activity, conclusions on self-similarity may exclude some subregions where strain rate directions are not consistent with expected directions, for example, in the NST region.

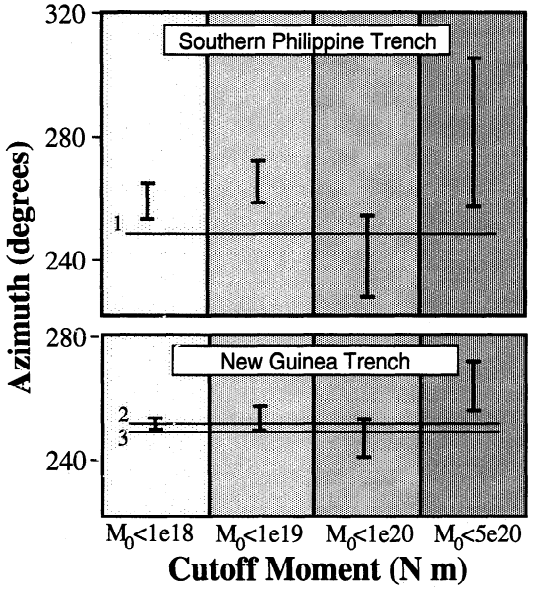

Figure 5. Error bars indicate the range of average azimuths of velocities along the southern Philippines Trench and New Guinea Trench estimated from seismic moment tensors for four windows with different cutoff moment magnitude. As a reference, azimuths of plate motion directions are given: 1, Philippine Sea-Australia [*DeMets et al.*, 1994]; 2, Caroline-Australia from *Seno et al.* [1993] and *DeMets et al.* [1994]; 3, Pacific-Australia [*DeMets et al.*, 1994].

The strain rate field (Figure 6a) is characterized by several types of strain:

1. low seismic strain is found along the Sunda-Banda arc. Together with the shortage of large historic events [*Pacheco and Sykes*, 1992], this low level of strain emphasizes that little seismic deformation has occurred this century along this arc, for both the Java Trench as well as the Timor Trough. The only significant seismic strain along the arc can be found in the back arc of the Timor Trough, along the Flores and Wetar thrusts.
2. low seismic strain is found along the NST. This is, however, only true for small, and moderate-sized events,

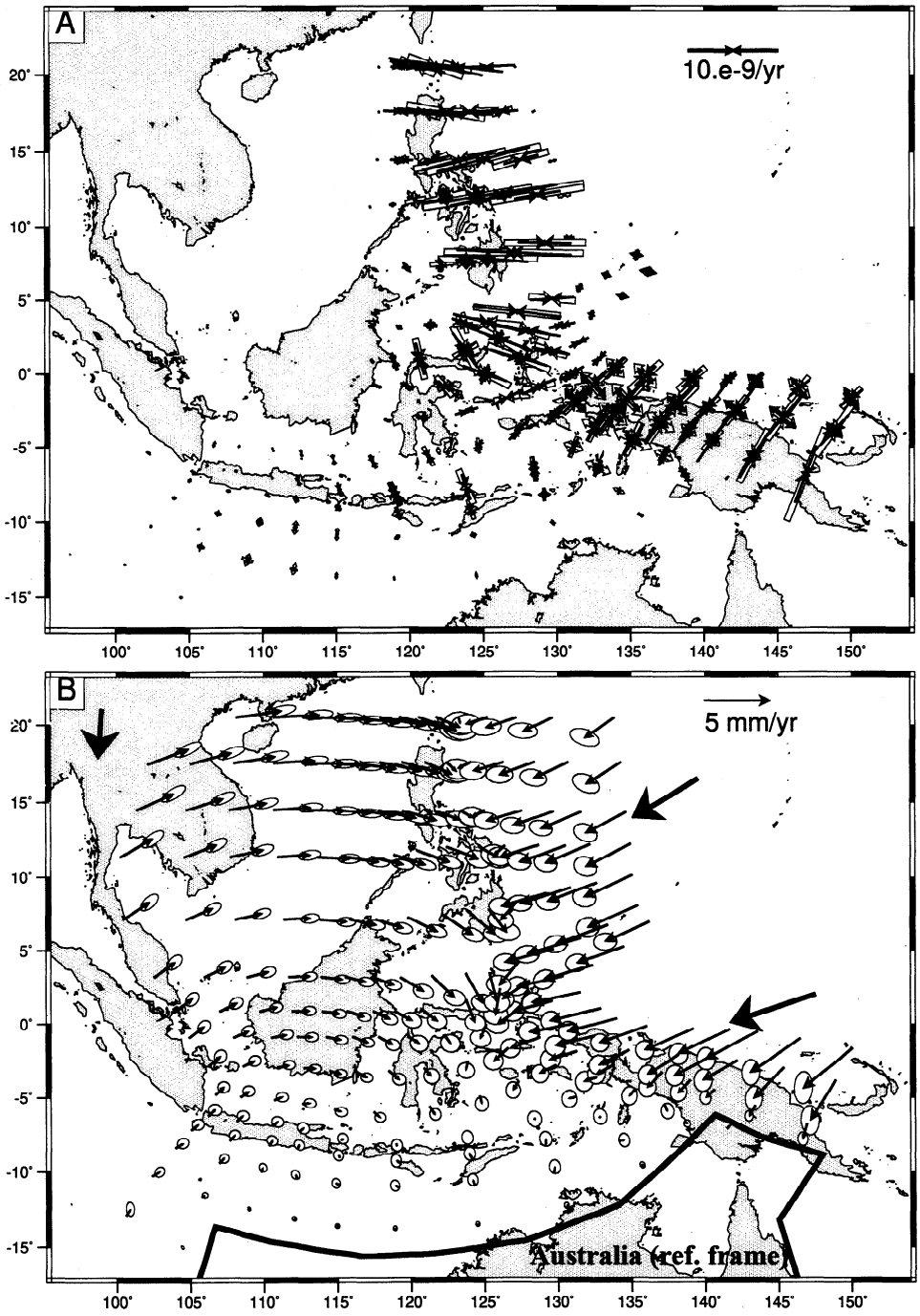

Figure 6. (a) Model strain rate field from an inversion of seismic strain rate tensors inferred using events with $M_0 < 1 \times 10^{20}$ N m. Strain rate solutions show principal axes of the observed average strain rates from earthquakes (open axes) and the model average principal strain rates (solid axes) for each area. (b) Model velocity field relative to Australia (outlined by thick black line). The three large arrows indicate the direction (not magnitude) of NUVEL-1A motions of the Pacific, Philippine Sea, and Eurasian plates relative to Australia [*DeMets et al.*, 1994]. Error ellipses represent one formal standard error, related to the assumption that seismicity follows a Poisson probability distribution. Hence the moment tensor $M_o m_{ij}$ of each earthquake makes a contribution of $\pm M_o m_{ij}$ to the uncertainties in strain rates.

because several large thrust events have occurred along this trench in recent times.

3) mainly pure convergent strains are found in the Philippines and Molucca Sea region. However, a significant number of strike-slip events are known to have occurred in the Philippines (*Pacheco and Sykes*, [1992], and Harvard CMT catalog).

4) a domination of strike-slip strain is found in western New Guinea, and NE-SW aligned convergent strain is found in the eastern part of the island. Convergent strain is notably absent along the NGT.

The velocity (Figure 6b) obtained from seismic moment tensors inferred from events with $M_0 < 1 \times 10^{20}$ N m shows the agreement in direction on the eastern part of the grid with

NUVEL-1A PH-AU and PA-AU relative motions (see also Figure 5), characteristic of all three windows below this magnitude cutoff. The absence of any significant seismicity along the Java Trench results in a poorly constrained motion for Sunda.

6. GPS Data

GPS data are taken from several studies [*Genrich et al.*, 1996; *Puntodewo et al.*, 1994; *Simons et al.*, 1999; *Kato et al.*, 1998; *Tregoning et al.*, 1998; *Stevens et al.*, 1999; *Yu et al.*, 1999], as well as from the International GPS Service (IGS) (epoch 1999.5), which can be downloaded from their website at http://sideshow.jpl.nasa.gov/mbh/series.html. The different campaigns are conducted in several (sub) regions (Figure 2), and the GPS velocities are shown in Figure 8c. Any station with a measurement that is reported to be affected by coseismic deformation or that shows a weak signal related to measurement irregularities is not used. We have taken out the measurement for the station at the island of Palau, which exceeds PH NUVEL-1A velocity by ~18% [*Kato et al.*, 1998]. This station was reported to have a large uncertainty due to the short analysis period [*Kato et al.*, 1998].

We acknowledge that formal errors in GPS velocities generally underestimate the "true" uncertainty and that this problem could also differ between different GPS campaigns depending on the length of the observation period. An accurate estimate of the "true" velocity uncertainty can be obtained not only by considering "white noise" in the analysis of the raw data but also by taking into account the effects of time-correlated noise [*Mao et al.*, 1999]. However we have no access to the raw data. Therefore, we multiply published standard errors by a conservative factor of 2, which should on average be sufficient as a close estimate of the "true" velocity uncertainty. The velocity of the IGS station in Singapore, however, is given an uncertainty that is 10 times higher than what is published, because of the short period over which this station is operational compared to other IGS stations that we use.

An initial inversion of the 93 GPS velocities is performed and a model velocity field relative to Australia (as defined in our grid, Figure 2) is obtained by a least squares fit to the data. In this procedure the reference frames of the individual GPS studies are not adopted, and instead they are left to be determined in the inversion. Following this procedure, a pole is obtained that rotates the IGS velocities located on the AU plate from the ITRF-96 reference frame to an Australian reference frame. We find the pole for this rotation (34.4°S, 136.5°W, 0.64° My^{-1}) (Table 1) to be a stable result. This pole differs from the NNR-NUVEL-1 pole for AU which is located at 33.8°S, 146.8°W with a rate of 0.68° Myr^{-1} [*Argus and Gordon*, 1991], indicating a possible discrepancy in the NUVEL-1/1A model [*DeMets et al.*, 1990, 1994] describing present-day AU motion (Table 1). This discrepancy has already been noted by others [e.g., *Larson et al.*, 1997]. Adopting our derived pole as a better estimate for AU-NNR motion, we use this pole to rotate the velocities by *Simons et al.* [1999], *Stevens et al.* [1999], *Tregoning et al.* [1998], and *Puntodewo et al.* [1994] into an Australian reference frame. All these studies are published in an ITRF reference frame, albeit not all in the same epoch. Assuming that NNR-NUVEL-1 accurately describes present-day Eurasia plate (EU) motion, as suggested by IGS velocities, we find a (new) AU-EU pole at 14.7°N, 48.8°E, with a rate of 0.69° My^{-1}, which is ~8° east of the NUVEL-1A estimate [*DeMets et al.*, 1994] (see Table 1). This pole is used to rotate the two velocities taken from *Kato et al.* [1998] from an Eurasian to an Australian reference frame. The reference frame for the velocities by *Genrich et al.* [1996] is left to be determined in the inversion, because velocities in that study were given in locally defined reference frames. The same is done for the velocities from *Yu et al.* [1999], because their velocities are referenced to only one station (Shanghai [*Heki*, 1996]), and thus their EU reference frame may be subject to some uncertainty.

7. Inversion of GPS Velocities With No Constraints From Seismicity

In the inversion procedure the 93 GPS velocities are matched while no a priori constraints are placed on the style and direction of the model strain rate field. The principal axes of the strain rate field and the velocity field for this isotropic case are shown in Figures 7a and 7b, respectively. The absence of constraints on the deformation results in high uncertainties in the model velocity field within the plate boundary zones (Figure 7b). These large uncertainties indicate that for this

Table 1. Relative Angular Velocities as Determined in This Study

Plate Pair	Latitude, °N	Longitude, °E	ω, ° Myr^{-1}
Australia - NNR (this study)	34.4	43.5	0.64
Australia - NNR [*Argus and Gordon*, 1991]	33.8	33.2	0.68
Australia - Eurasia (this study)	14.7	48.8	0.69
Australia - Eurasia [*DeMets et al.*, 1994]	15.1	40.5	0.69
Sunda - Eurasia (this study)	-25.3	131.9	-0.24
Sunda - Eurasia (this study)[a]	-29.5	139.0	-0.21
Sunda - Eurasia (this study)[b]	-29.9	137.6	-0.21
Sunda - Eurasia [*Simons et al.*, 1999]	-31.8	134.0	-0.28

Angular velocities are for the first plate relative to the second. NNR, No-net-rotation [*Argus and Gordon*, 1991].

[a] In this model no a priori constraints on the style and direction of the model strain rate field are used.

[b] In this model the reference frame for all GPS studies used in this study are left undefined prior to the inversion and are instead determined in the inversion procedure.

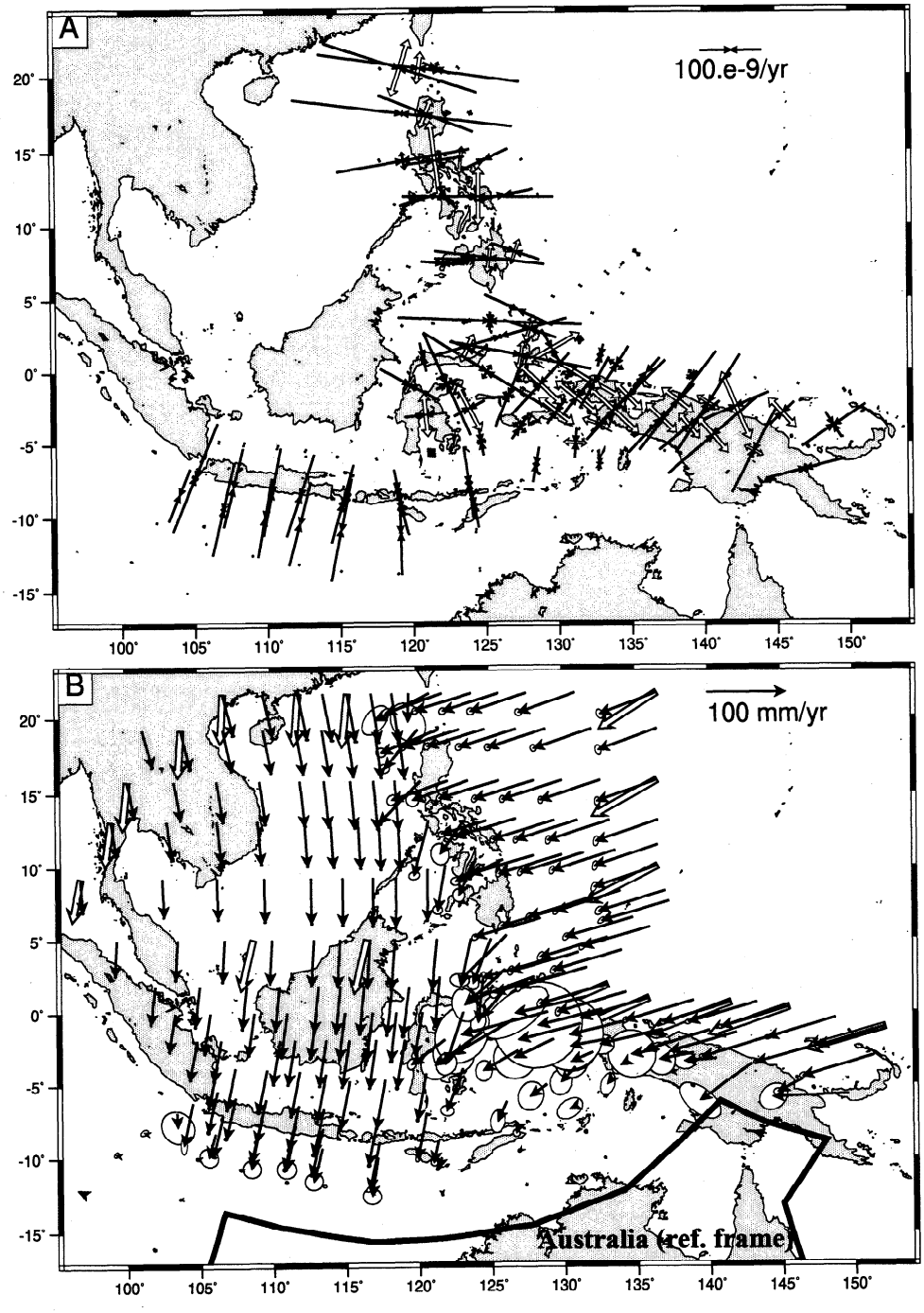

Figure 7. (a) Principal axes of model strain rates obtained from fitting GPS velocities (see Figure 2 and text for data sources). Open arrows indicate extensional strain rates, and solid arrows correspond to compressional strain rates. For this solution no information about the style and direction of deformation within areas is taken into account (i.e., the areas are considered to behave isotropically). (b) Model velocity field relative to Australia obtained from fitting GPS velocities. Error ellipses represent 1σ standard error. Open vectors indicate NUVEL-1A motions of the Pacific and Philippine Sea plate relative to Australia [*DeMets et al.*, 1994], as well as Eurasia-Australia motion obtained from our derived pole of rotation for this plate pair (see Table 1).

study, with a poor site coverage at some places, the GPS data alone do not uniquely define a reliable long-term strain rate field. The average weighted misfit of the model velocity field to the observed GPS velocities is given in Table 2. In some areas the model strain rate field (Figure 7a) has a rapid spatial variation in style and direction from one grid area to another (e.g., the northern Sulawesi - Molucca Sea region). There are some clear differences between the seismic strain rate field (Figure 6a) and the model strain rate field derived solely from GPS observations (Figure 7a). These differences are the low seismic strain rates along the Java Trench, Palu Fault, and Manila Trench versus the high strain rates for these areas in the solution obtained from the interpolation of GPS velocities (Figure 7a). Also, GPS observations constrain a significant

Table 2. Goodness of Fit of Model Velocity Field to Geodetic Velocities, and Resolution of Model

	Unweighted		Weighted		
Model[a]	SSM	RMS	SSM	RMS	Resolution[b] (%)
A	211.3	1.19	156.8	0.88	80.2
B	206.4	1.16	178.7	1.00	87.2
C	123.5	0.69	331.9	1.86	71.0
D	142.5	0.80	114.1	0.64	68.5

SSM is the squared misfit between the model and observed velocity components. The average RMS misfit is calculated as the total SSM divided by the total number of matched velocity components (2×89). The four velocities on stable Australia from the International GPS Service (IGS) are not used, because, although the model velocities at these stations yield a perfect fit to the data, the very small uncertainties in these data cause a misleading large misfit. This reduces the number of velocities used in this analysis to 89. Result is shown for a case when the SSM and RMS are weighted by variances in the observed velocity components, and for a case when no such weighting has been applied.

[a] Model A is an inversion of GPS velocities with no constraints from seismicity. Model B is an inversion of GPS velocities using style and direction of seismic strain rate tensors to constrain the predicted strain rate field. Model C is the same as model B but with the original uncertainties in the GPS observations, where in models A and B those uncertainties were multiplied by a factor of 2 to acknowledge the general underestimation of the "true" uncertainty by observation uncertainties. Model D is the same as model B except that all GPS studies were not, a priori, tied in a defined reference frame; instead, reference frames were determined in the inversion.

[b] Resolution values are given by $1-[\sum_1^N (V_{\phi\phi}^m + V_{\theta\theta}^m + 2V_{\phi\theta}^m)]/[\sum_1^N (V_{\phi\phi}^o + V_{\theta\theta}^o + 2V_{\phi\theta}^o)]$, where the terms in parentheses are the trace elements of the covariance matrix of the model velocity at the position of the ith GPS observation (with superscript m) and of the covariance matrix of the GPS velocity at that location (with superscript o).

component of the strain rate field in the Philippines to involve strike-slip deformation, whereas the seismic strain rate field for this region is mainly dominated by convergent strain rate (Figure 6a). A detailed description of the model strain rate field is given in section 8, when constraints from seismicity are applied.

The velocity field shows that the predicted velocities are generally not in agreement with the NUVEL-1A model for the PH and PA plates [*DeMets et al.*, 1994], within a 2σ uncertainty (Figure 7b). Note that Sunda does not move in the expected direction of EU-AU motion, which indicates the independent motion of Sunda relative to EU.

8. Inversion of GPS Velocities With Constraints From Seismicity

In this section we combine the strengths of the seismicity and GPS data to obtain a best estimate of the long-term strain rate field. The result of the self-similarity test provides some confidence limits on the style and location of deformation, and we use information about the style and direction (but not the magnitude or sign) of the seismic strain rate field inferred from earthquakes with $M_0 < 1\times10^{20}$ N m to help constrain the model strain rate field in the inversion of GPS velocities.

As we demonstrated in section 5, it is generally not appropriate to use the population of events with $M_0 > 1\times10^{20}$ N m, because the number of events above this moment is too low to provide a statistically reliable estimate of the style of seismic strain rate. Although it is formally correct to exclude these 12 largest events when trying to infer the style and direction of the strain rate tensor field, for the purpose of testing model sensitivity we also investigate the effects of including these events. For this analysis the observed seismic strain rates are not smoothed. We find no significant difference in the style and direction of the predicted strain rate field and associated velocity field between a solution constrained by events with $M_0 < 1\times10^{20}$ N m or a solution constrained by events in the entire catalog. In section 8.1, however, we present results associated only for the model in which events with $M_0 < 1\times10^{20}$ N m are used to provide a priori constraints on the style and direction of strain.

8.1. The Model Strain Rate Field and Velocity Field

The model strain rate field and velocity field resulting from bicubic Bessel interpolation of GPS velocities with a priori constraints on the style and direction of the model strain rate field from earthquakes with $M_0 < 1\times10^{20}$ N m are shown in Figures 8a and 8b, respectively. Although a larger misfit between the model and observed velocities is obtained for the constrained case in comparison with the unconstrained case (Table 2), uncertainties in the predicted velocity field in the plate boundary zones (Figure 8b) are significantly lower than those in the unconstrained case (Figure 7b). This emphasizes the higher reliability of this estimate of the long-term strain rate field. This is also apparent from the strain rate field (Figure 8a), which shows a less rapid spatial variation in direction, style, and magnitude from one grid area to another (e.g., the Sulawesi-Molucca Sea region) in comparison with the unconstrained strain rate field (Figure 7a).

The velocity of PH relative to AU (Figure 8b) is closer to the NUVEL-1A estimate than it is in the solution with no constraints on deformation style and direction (Figure 7b). A PH-AU velocity with an azimuth that is slightly clockwise of the NUVEL-1A PH-AU velocity (Figure 8b) is consistent with findings by *Kato et al.* [1998]. However both in this study and in that by Kato et al. only one station is used to constrain PH motion. Velocity directions relative to Australia are in accord with NUVEL-1A relative motion for the Pacific plate, but velocity magnitudes are about 8 mm yr^{-1} slower than the NUVEL-1A estimate. The directions for PA-AU and PH-AU relative motions are consistent with the directions in the velocity field associated with seismic moment release with $M_0 < 1\times10^{20}$ N m (Figure 6b). The differences in PA and PH motion between the unconstrained and constrained cases (Figures 7b and 8b) relate to differences in the respective strain rate fields in the Philippine and New Guinea regions (compare Figures 7a and 8a). For other regions (e.g., the Java Trench, where seismic strain is low and is consequently not used to constrain the total strain rate field), the velocity field and strain rate field (Figures 8a and 8b) are almost identical with the unconstrained solution (Figures 7a and 7b).

There are large, convergent strain rates south of Java, along the Java Trench (Figure 8a), which is directly related to the accommodation of ~70 mm yr^{-1} of shortening between Java and the Christmas and Cocos Islands as inferred from the GPS measurements [*Genrich et al.*, 1996; *Simons et al.*, 1999]. The eastern Banda arc exhibits large convergent strain in the back arc and Banda Sea region, and there is no indication of active

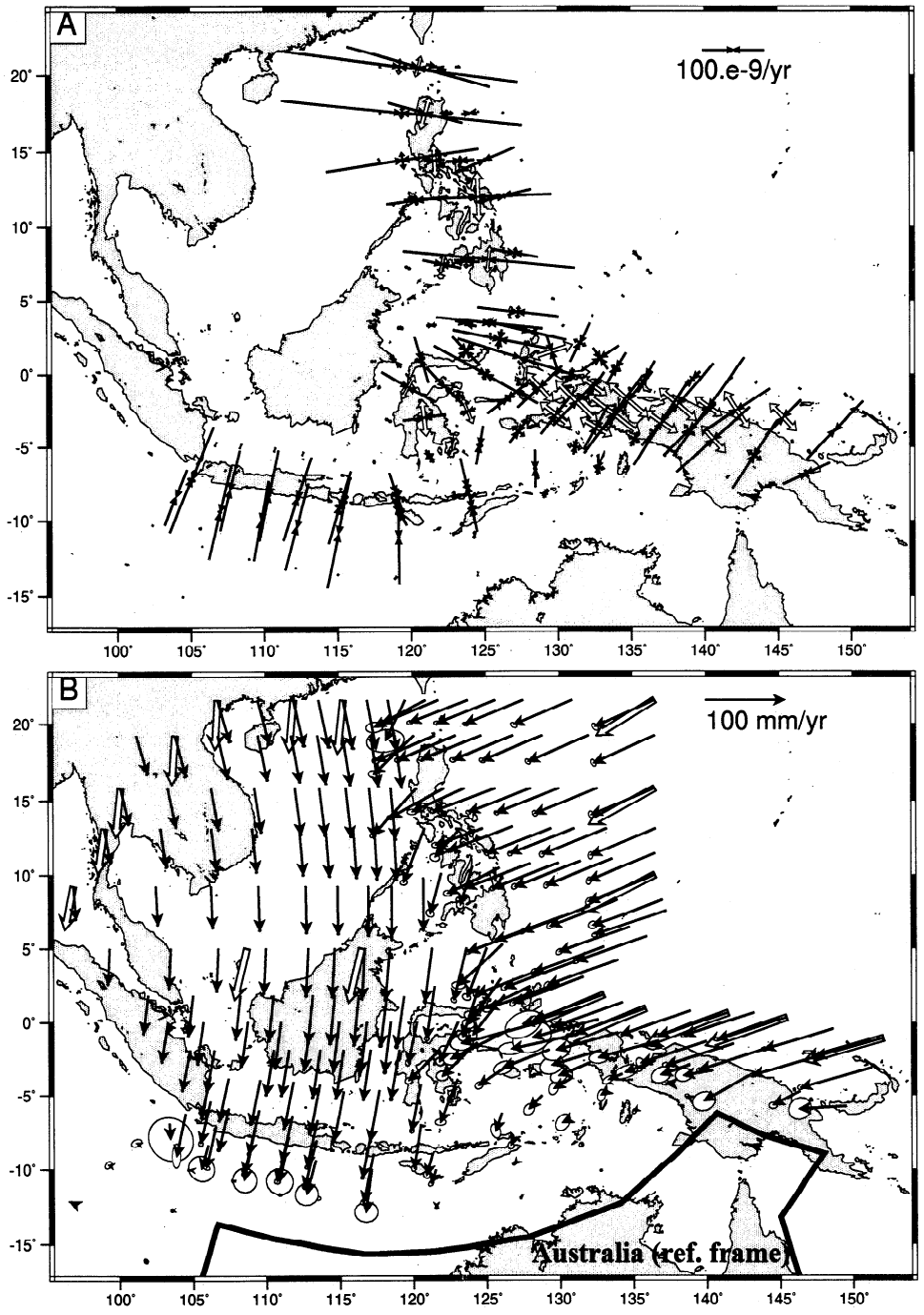

Figure 8. (a) Principal axes of model strain rate field obtained from fitting GPS velocities. Open arrows indicate extensional strain rates, and solid arrows correspond to compressional strain rates. Directional information of the principal strain rates (±10° uncertainty) is inferred from the seismic strain rate tensor field associated with events for which $M_0 < 1 \times 10^{20}$ N m (Figure 6a). These events are also used to constrain the style (but not magnitude) of strain rate tensor (corresponding to equivalent of dip-slip, strike-slip, or mixed style). (b) Model velocity field relative to Australia obtained from fitting GPS velocities with a priori information on the style and direction of the strain rate field. Error ellipses represent 1σ standard error. Open vectors indicate NUVEL-1A motions of the Pacific and Philippine Sea plate relative to Australia [*DeMets et al.*, 1994], as well as Eurasia-Australia motion obtained from our derived pole of rotation for this plate pair (see Table 1).

deformation along the Timor Trough. This is consistent with earthquake occurrence patterns. The absence of active deformation along the Timor Trough near the Island of Timor has already been noted by *Genrich et al.* [1996] from GPS observations. The absence of active deformation near Timor was also noted by, for example, *Audley-Charles* [1986] and *Snyder et al.* [1996], on the basis of seismic reflection profiles. However, their conclusion is in disagreement with a study by *Karig et al.* [1987], also based on seismic profiling, which concluded that some active deformation is still

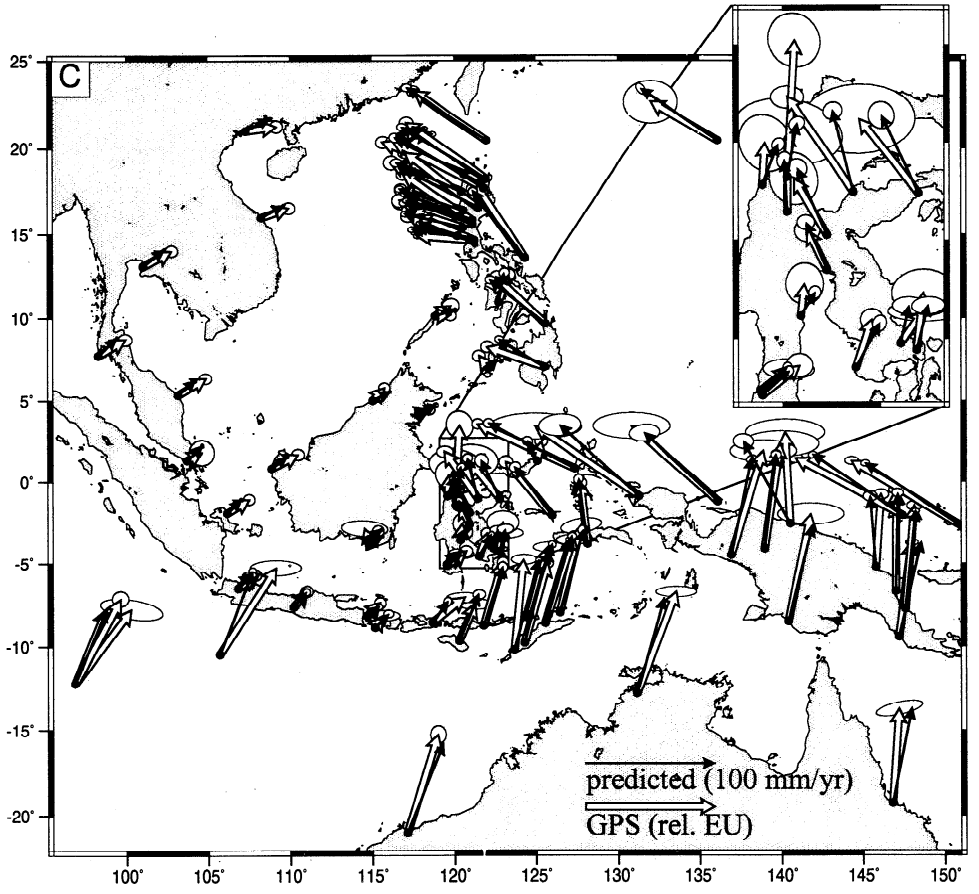

Figure 8c. GPS observations (open vectors) and our predicted velocity field (solid vectors) in a Eurasia (EU) reference frame. (We used our determined Australia-Eurasia pole of rotation (Table 1) to rotate the solution in Figure 8b into a Eurasia reference frame). Inset gives velocities in Sulawesi on a scale twice as large as that in the main map. Error ellipses represent 1σ standard error. However, for the observed velocities these uncertainties actually reflect 2σ standard error, because prior to the inversion standard errors of GPS velocities are multiplied by a factor 2 to acknowledge possible uncertainty underestimations in the GPS observations. The velocities for the four IGS stations in southern Australia are not shown.

occurring there. Our result indicates a jump in convergence along the Banda arc from the Java Trench to the back arc in the more eastern arc, as recognized by others [e.g., *McCaffrey*, 1988; *Audley-Charles*, 1975]. This jump can also be seen in the dilatational strain field (Figure 9a) associated with the result in Figure 8a. Our result thus confirms the cessation of subduction at the Timor Trough proposed *by Johnston and Bowin* [1981] and *Charlton* [1986] and suggests that the southern Banda arc east of Sumba is part of the Australian plate.

Southern New Guinea shows little deformation and is therefore, like the eastern Banda Sea and eastern Banda arc, essentially part of the Australian plate (Figures 8a and 9). A profound E-W striking zone of strike-slip deformation dominates northern New Guinea, clearly seen in the shear strain rate field (Figure 9b), with a maximum in shear strain rate in west New Guinea between the Tarera-Aiduna and Sorong Faults. North of eastern New Guinea, strike-slip deformation is dominant, consistent with earthquake occurrence and the seismic strain rate field (Figure 6a). North of western New Guinea, along the NGT, convergence is dominant but occurs at a relatively low rate. The partitioning of the oblique convergence between the PA and AU plates in trench-normal convergence and strike-slip-dominated deformation (mixed with thrusting) south of the trench (Figures 8a and 9) is not explicitly present in the seismicity data used to constrain the deformation (Figure 6a). In particular it is important to note that the principal strain rate axes along the NGT (Figure 8a) are consistent with the mechanism of the 1996 Biak event ($M_w = 8.2$) [e.g., *Okal*, 1996] (Figure 3), although this event was not used to constrain the style of the model strain rate field, because of its large size. Thus the style of the Biak event (pure thrust) was expected and consistent with the oblique relative plate motion. On the other hand, our analysis shows that the large magnitude of the Biak event is expected to be rare, considering the relatively low magnitude of model strain rate along the NGT.

Along the Philippine Trench almost pure convergent strain rates are present (Figures 8a and 9a). Strain rate tensors west of the trench, however, show significantly higher convergence than along the trench. This strain rate west of the trench also exhibits a significant strike-slip component (Figures 8a and 9b), which indicates strain partitioning to accommodate PH-Sunda motion. However, although numerous strike-slip events are known to have occurred on the Philippine islands, the significant strike-slip component is not apparent from the seismic strain rate field for $M_0 < 1 \times 10^{20}$ N m (Figure 6a). Thus GPS velocities are providing that information. Some

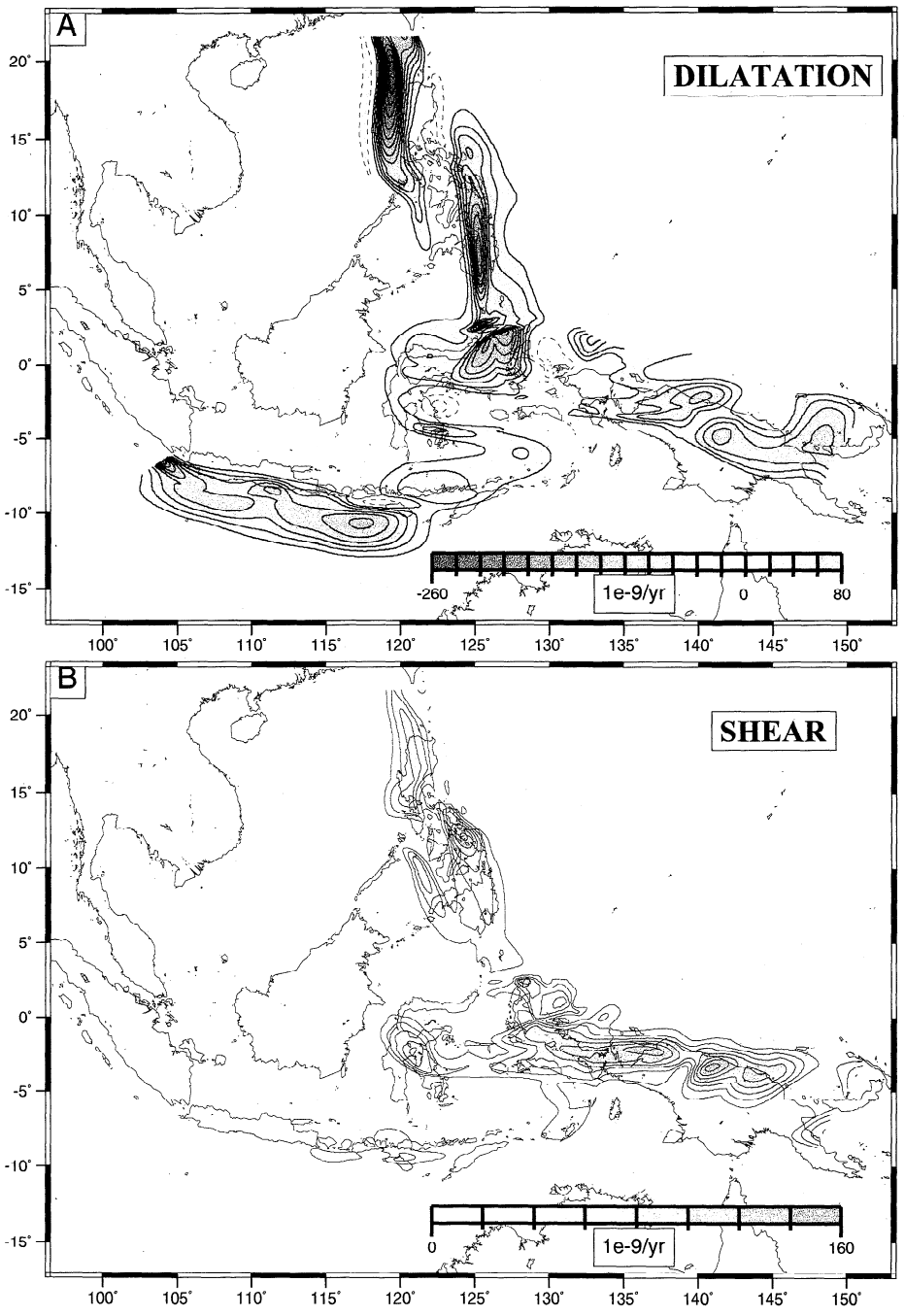

Figure 9. (a) Dilatational strain rates for the solution in Figure 8a. Shade and contour interval is 20×10^{-9} yr^{-1}. Negative strains (compression) are contoured with solid lines, and positive strains (extension) are contoured with dashed lines. (b) Shear strain rates (associated with pure strike-slip faulting) for the solution in Figure 8a. Shade and contour interval is 20×10^{-9} yr^{-1}.

convergence as well as shear is taken up along fault zones west of the southern archipelago, like the Negros and Cotabato Trenches and Cotabato Fault, but this is relatively minor compared to convergence east of these trenches (Figures 8a and 9a). For the northern Philippines, PH-Sunda motion is accommodated primarily along the Manila Trench west of the Philippines, with only a small amount occurring along the East Luzon Trough (Figures 8a and 9a). The large predicted convergence rates along the Manila Trench indicate the importance of this trench as a zone of convergence, which is in agreement with, for example, the independent study by *Rangin et al.* [1997] based on GPS measurements as well as the observation of active deformation along this margin inferred from seismic profiles [*Hayes and Lewis*, 1984].

There are high convergent strain rates predicted for the Molucca Sea region and along the NST. This prediction indicates the relative importance of these regions as zones of shortening, where the NST probably accommodates some of the distributed AU-Sunda motion.

An interesting detail is the high predicted shear strain in central Sulawesi (Figure 9b) in a zone that is more or less parallel to the Palu Fault (Figure 1). From existing seismicity

catalogs (e.g., CMT and *Pacheco and Sykes* [1992]), *Walpersdorf et al.* [1998] inferred that no event larger than M_W = 4.5 has occurred on this fault in the last century. The observed importance of this region in our result is consistent with the conclusions of Walpersdorf et al.. Based on a subset of the GPS velocities used in this study, they infer a minimum strike-slip displacement rate along the Palu Fault of 30 mm yr^{-1}, which has probably accumulated to at least 3 m over the last 100 years. Given the dimensions of the fault, this would imply a potential M = 7 earthquake [*Walpersdorf et al.*, 1998].

8.2. Model Sensitivity

We perform a test to determine the resolution of our model by comparing the covariance matrix of the GPS velocities with the covariance matrix of the model velocity field at the locations of the GPS observations (Table 2). The resolution increases significantly when constraints on the style and direction of the predicted strain rate tensor field are applied (model B, Table 2).

We also conduct a statistical test in order to understand the influence of the assigned uncertainty in the GPS observations. In this test, GPS velocities are given their original standard errors, instead of uncertainties used in our model that are twice as large as published uncertainties. The result (model C, Table 2) indicates that GPS observations can be matched better when original standard errors are adopted than in our preferred model. However, if the sum of squares is weighted by the variances in the observed velocities, a large weighted misfit becomes apparent in model C. There is also a lower degree of resolution in the model velocity field for model C. We also test the effect of the constraint of reference frames. In this test we do not constrain any GPS velocity, a priori, to a specific reference frame. Instead, we leave the reference frames of all studies to be determined in the inversion. Although a better fit is obtained to the GPS velocities for this case (model D, Table 2), we do not regard the improved fit to be significant enough to justify a better solution. The reason for this is that some information related to global plate motions, imbedded in the GPS studies that are linked to global stations in an ITRF reference frame, may be lost when reference frames are solved for (unless the grid is sufficiently large to include many plates on the Earth's surface). Furthermore, note also the significantly lower resolution of the model velocity field when reference frames are not defined a priori (model D, Table 2).

9. Total Predicted Scalar Moment Rates Versus Seismic Scalar Moment Rates

To compare the seismic moment release rate with the moment release rate inferred from our estimate of the total long-term strain rate field (Figure 8a, Table 3), we compile all events with M > 7 from 1963-1996 from the Harvard CMT catalog and *Pacheco and Sykes* [1992]. As this period is too short to capture the complete seismic cycle of the largest events (as is also indicated by our self-similarity tests of the CMT catalog in section 5), the comparison will only yield an estimate of the current differences between seismic and total strain rate and will not yield an estimate of the long-term seismic versus aseismic strain rate.

We calculate the seismic moment release for several subregions (Figure 10). On average, for all the active zones in the region, the seismicity in the period of the catalog represents only ~40% of the moment release expected on the

Table 3. Predicted Strain Rates for Specified Regions, Minimum Moment Release Rates Associated With Horizontal Strain Rate Tensors From Our Model, and Seismic Moment Rates From Events With M > 7 Between 1963 and 1996

			Model			
Area in Figure 10	Region	Area, 10^5 km^2	Strain Rate[a]	Minimum Moment Rate[b]	Seismic Moment Rate	Seismic/Model, %
A	Java Trench	7.82	16.0	23.5	1.6/12.1[c]	7/51[c]
B	Flores-Wetar Thrusts	2.24	1.6	3.9	1.6	41
C	Banda Sea	3.78	1.9	3.9	0.0	0
D	Sulawesi (Palu Fault)	1.29	1.7	2.2	0.0	0
E	North Sulawesi Trench	1.81	1.6	2.3	4.3	187
F	Molucca Sea	1.59	5.5	6.4	1.6	25
G	Seram Trough	1.64	2.4	2.7	7.1	263
H	New Guinea	4.93	9.4	13.0	1.9	15
I	New Guinea Trench	3.72	7.1	7.4	7.1	96
J	western Philippines	2.93	2.0	3.7	5.7	154
K	Philippine Fault	3.64	6.9	10.7	1.6	15
L	Philippine Trench	1.49	2.7	4.8	5.2	108
M	Manila Trench	1.22	6.3	8.1	0.1	1
N	East Luzon Trough	1.02	0.6	0.7	1.4	200

Seismic moment rates are inferred from the Harvard centroid moment tensor catalog and *Pacheco and Sykes* [1992]. Units for model moment rates and seismic moment rates are 10^{19} N m yr^{-1}.

[a] Strain rate is defined as the sum of dilatation strain rate and principal shear strain rate, $0.5|\dot{\varepsilon}_{xx} + \dot{\varepsilon}_{yy}| + \sqrt{0.25(\dot{\varepsilon}_{xx} - \dot{\varepsilon}_{yy})^2 + \dot{\varepsilon}_{xy}^2}$. Units are in 10^{-7} yr^{-1}.

[b] Minimum moment rate is equal to $2\mu V(0.5|\dot{\varepsilon}_{xx} + \dot{\varepsilon}_{yy}| + \sqrt{0.25(\dot{\varepsilon}_{xx} - \dot{\varepsilon}_{yy})^2 + \dot{\varepsilon}_{xy}^2})$, where $\mu = 3.5\times10^{10}$ N m^{-2} is the shear modulus, V is the volume, which is the product of the area of the region and the seismogenic depth, which is assumed to be 30 km.

[c] First value is associated with a seismic catalog without the 1977 Sumba event (M_W = 8.3).

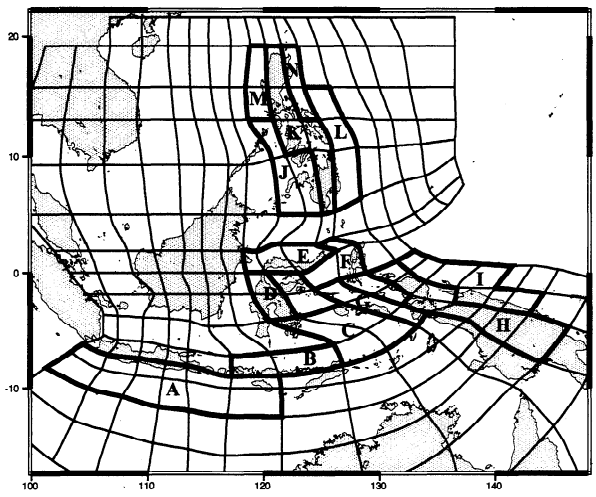

Figure 10. Areas for which a seismic scalar moment release rate versus the minimum scalar seismic moment release rate is calculated (see Table 3). A, Java Trench; B, Flores-Wetar Thrusts; C, Banda Sea; D, Sulawesi-Palu Fault; E, North Sulawesi Trench; F, Molucca Sea; G, Seram Trough; H, New Guinea Thrust Belt; I, New Guinea Trench; J, western Philippines; K, Philippine Fault; L, Philippine Trench; M, Manila Trench; N, East Luzon Trough.

basis of our total deformation field. Regions with a relative underrepresentation of seismic activity like the Java Trench and the Banda Sea can be identified. This deficit could be related to geodynamic processes related to the arc-continent collision between Australia and the Banda arc and the possible adjustment of the northern Australian plate boundary, or to the short period of seismic data. *Scholz and Campos* [1995] have suggested that relatively low coupling should exist for the Java subduction zone owing to the slab pull force, which has a tendency to reduce the force normal to the subduction thrust interface. Low seismic coupling for this region was also suggested by *Pacheco et al.* [1993] on the basis of the seismic catalog for the twentieth century [*Peterson and Seno*, 1984; *Pacheco and Sykes*, 1992], but as was shown by *McCaffrey* [1997], such conclusions are unreliable given the shortness of seismic record. *Newcomb and McCann* [1987] found that several major earthquakes occurred along the Java Trench in the nineteenth century; however, it could be that these earthquakes were intraplate events. Newcomb and McCann also present evidence of active deformation in the forearc from other geophysical data and concluded that most of the deformation occurs aseismically.

Regions such as the NST, western Philippines, Seram Trough, and East Luzon Trough exhibit relatively large seismic strain. The surplus of seismic moment release along the latter two can largely be attributed to the contribution of a single large event for each region: the 1965 Ceram Sea event (M_w = 8.2) and the 1968 Luzon event (M_w = 7.8), respectively. These regions with a seismic moment release rate that is significantly larger than our predicted moment rate emphasize once again that the seismic catalog is too short to reflect the long-term rate of seismic strain release.

Seismic moment release along the Manila Trench can be attributed solely to a large strike-slip event (M_w = 7.1) that occurred in 1972 [*Pacheco and Sykes*, 1992] and which may be unrelated to the subduction process at the trench. Several large thrust events have occurred beneath northern Philippines at depths greater than 30 km, and it is not clear whether they can be associated with subduction of the Manila slab. Furthermore, the two large events that are known to have occurred along the western margin of the northern Philippines during this century (M = 7.6 in 1934 and M = 7.2 in 1948) have no determined mechanisms [*Cardwell et al.*, 1980; *Hamburger et al.*, 1983]. In part on the basis of the general low level of seismicity along this margin, *Seno and Kurita* [1978] and *Rowlett and Kelleher* [1976] proposed that subduction at the Manila Trench has ceased, or at least slowed down significantly. Our analysis shows a high predicted strain rate along the Manila Trench. Most likely, a large portion of this strain rate is accommodated aseismically, but given the exceptionally high rate of strain, a significant potential earthquake hazard may exist. However, we emphasize again that a much longer earthquake catalog is needed to make more conclusive inferences [*McCaffrey*, 1997].

10. Predicted Velocity Field Versus Plate Motions

Potential differences between the predicted velocity field on the stable plates and NUVEL-1A relative motions point out discrepancies between geodetic observations and plate motions. These discrepancies may be caused by plate motion adjustments over the last 3 Myr (i.e., the time interval for which NUVEL-1A is an estimate). Alternatively, differences between our model plate velocities and NUVEL-1A estimates may reflect an inadequate coverage of GPS observations on the stable portions of the PA and PH plates covered in our model. However, we find that there is only a minor difference between the present-day motions inferred from GPS data and the NUVEL-1A plate motion estimate for this region (Figure 8b).

The discrepancy between EU-AU NUVEL-1A relative motion and our predicted velocity for the western part of the grid (Figure 8b) indicates independent motion of Sunda with respect to stable EU, which was first proposed by *Cardwell and Isacks* [1978]. Solely on the basis of the GPS observations from the "GEODYnamics of South and South-East Asia" (GEODYSSEA) project, others obtained a Sunda-EU pole at 32°S, 134°E at a rate of -0.28° Myr^{-1} [*Simons et al.*, 1999; *Chamot-Rooke et al.*, 1997]. We also solve for the rotation vector of Sunda as it is defined in our grid to determine the Sunda-EU rotation pole at 25°S, 132°E, -0.24° Myr^{-1}. (Poles of rotation are summarized in Table 1.) Although we consider more GPS observations and use a technique different from *Simons et al.* [1999] and *Chamot-Rooke et al.* [1997] to derive poles of rotation, our result and their pole estimate are within 1σ. Both their study and this study confirm clockwise rotation for Sunda-EU relative motion, which results in a NE to ENE motion of Sunda at ~16-21 mm yr^{-1} relative to EU (Figure 8c). The difference in pole position leads to a direction that is ~4° more northward for our predicted solution than for the GPS observations. Earlier, *Ren et al.* [1997] showed that on the basis of kinematic modeling of central and Southeast Asia using geodetic, geologic, and seismicity data, Sunda moves eastward relative to EU at ~10-15 mm yr^{-1}, but their block motion was about a pole of rotation far to the north (62°N, 132°E, 0.14° Myr^{-1}). The result of the high predicted subduction rate of Sunda at the Manila Trench and the slab pull forces that accompany this may explain, in part, the clockwise rotation and eastward motion of Sunda relative to EU.

For completeness, Table 1 also contains the Sunda-EU poles of rotation for the case where GPS velocities are inverted without constraints from seismicity and for a case without the a priori definition of the reference frames for the individual GPS studies. For all cases we find a significant Sunda-EU motion that is roughly similar.

Weissel and Anderson [1978] proposed the presence of an independent Caroline plate. The relative velocity for Caroline-AU motion is ~1°-4° clockwise from the direction of the NUVEL-1A PA-AU estimate [*Seno et al.*, 1993; *DeMets et al.*, 1994]. Our result agrees with the NUVEL-1A PA-AU motion direction (Figure 8b). The 1°-4° difference between the motion of the two plate pairs falls, however, within the 2σ uncertainty. Expected Caroline-AU motion is 5-6 mm yr^{-1} faster than NUVEL-1A PA-AU motion [*Seno et al.*, 1993; *DeMets et al.*, 1994]. Our model velocities at this margin are ~8 mm yr^{-1} slower than NUVEL-1A PA-AU motion. *McCaffrey* [1996] concluded that on the basis of earthquake fault plane solutions, PA and Caroline plate motions are indistinguishable. Given the fact that we do not include GPS velocities measured on the Pacific (Caroline) plate, we can not make conclusive inferences on the existence of an independent Caroline plate from our model velocity field.

11. Conclusions

The eastern Indonesia and Philippines region contains a variety of complex plate boundaries. GPS and seismicity data can provide information about the style and distribution of the long-term strain rate tensor field in this region. We find that the style and direction of the seismic strain rate tensor field based on earthquakes from the Harvard CMT catalog are roughly self-similar over at least 2 orders of magnitude, up to $M_0 = 1 \times 10^{20}$ N m. The CMT catalog is too short to obtain a statistically reliable estimate of the relative contribution of the largest events to the total seismic strain rate field. The largest events (except for the 1977 Sumba, M_w = 8.3) are, however, consistent in style with the strain rate field derived from small, and medium-sized events. We show that GPS measurements, by themselves, are not sufficient to provide a reliable estimate of the style, direction, and location of the strain rates within the boundary zones. Our best estimate of the first-order, long-term strain rate tensor field for the entire region combines the strengths of the GPS and seismicity data. For our final model we use the style and direction of the strain rate field inferred from earthquakes with $M_0 < 1 \times 10^{20}$ N m as a constraint in the inversion of GPS velocities for a self-consistent velocity and strain rate field.

Predicted velocities for the stable surrounding plates are in good agreement with the NUVEL-1A model, except for the Sunda block, which is explained by the established idea that Sunda is an independent entity from stable Eurasia [e.g., *Cardwell and Isacks*, 1978; *Johnston and Bowin*, 1981]. Our self-consistent model strain rate field (Figure 8a) indicates strain partitioning for the Philippines. The model shows a significant amount of strike-slip strain rate along the Philippine Fault. Furthermore, rates of convergence are higher at the Manila Trench than along the Philippine and East Luzon Trenches. This result indicates the importance of the Manila Trench in accommodating PH-Sunda motion, which is not evident from the relatively low level of seismicity along this trench. Strain partitioning also occurs in western New Guinea; however, the trench-normal component is small, and most deformation is taken up in an E-W trending zone of almost pure strike-slip deformation, consistent with seismicity occurrence. The Java Trench clearly delineates the Sunda-AU boundary, although this trench has not been associated with a high level of seismicity in the last 100 years. East of Sumba, Sunda-Australia motion is accommodated mostly within the back arc of the Banda Arc and the eastern Banda Sea region. This indicates the absence of subduction along the Timor Trough and suggests that the southern Banda arc that lies east of Sumba, as well as the eastern Banda Sea, is part of the Australian plate. Along the North Sulawesi Trench there is a significant amount of shortening in a direction similar to that of Sunda-Australia motion, indicating that this area is part of the diffuse plate boundary zone between Australia and Sunda. Although seismicity delineates most of the plate boundary zones in the region, the relative importance of some parts of the plate boundary zones, like the Java and Manila Trenches, is not necessarily associated with the high moment release of large earthquakes. This could be either due to the shortness of the catalog or due to the aseismic deformation associated with geodynamic processes that cause decoupling.

Acknowledgments. We thank Boudewijn Ambrosius and Andrea Walpersdorf for providing GPS data before publication and Tim Dixon, Michael Hamburger, and Eli Silver for constructive reviews. We also thank Marleen Nyst for help and discussion on the GEODYSSEA data. Maps were drawn using GMT 3.0 [*Wessel and Smith*, 1991]. W.E.H. is supported by NSF grant EAR-9628872. This is a contribution of the Vening Meinesz School of Geodynamics.

References

Abers, G., and R. McCaffrey, Active deformation in the New Guinea fold-and-thrust belt: Seismological evidence for strike-slip faulting and basement-involved thrusting, *J. Geophys. Res.*, 93, 13,332-13,354, 1988.

Amelung, F., and G. King, Large-scale tectonic deformation inferred from small earthquakes, *Nature*, 386, 702-705, 1997.

Argus, D.F., and R.G. Gordon, No-net-rotation of current plate velocities incorporating plate motion model NUVEL-1, *Geophys. Res. Lett.*, 18, 2039-2042, 1991.

Audley-Charles, M.G., The sumba fracture: a major discontinuity between eastern and western Indonesia, *Tectonophysics, 26*,213-228, 1975.

Audley-Charles, M.G., Rates of Neogene and Quaternary tectonic movements in the southern Banda Arc based on micropaleontology, *J. Geol. Soc. Lond., 143*, 161-175, 1986.

Barrier, E., P. Huchon, and M. Aurelio, Philippine Fault: A key for Philippine kinematics, *Geology*, 19, 32-35, 1991.

Cardwell, R. K., and B. L. Isacks, Geometry of the subducted lithosphere beneath the Banda Sea in eastern Indonesia from seismicity and fault plane solutions, *J. Geophys. Res., 83*, 2825-2838, 1978.

Cardwell, R.K., B.L. Isacks, and D.E. Karig, The spatial distribution of earthquakes, focal mechanism solutions, and subducted lithosphere in the Philippine and northeastern Indonesian islands, in *The Tectonic and Geologic Evolution of Southeast Asian Seas and Islands*, Geophys. Monogr. Ser., vol. 23, edited by D.E. Hayes, pp.1-35, AGU, Washington, D.C., 1980.

Chamot-Rooke, N., C. Vigny, A. Walpersdorf, X. Le Pichon, P. Huchon, and C. Rangin, Sundaland motion detected from GEODYSSEA GPS measurements: Implications for motion at Sunda trenches, *Eos Trans. AGU, 78*(46), Fall Meet. Suppl., F169, 1997.

Charlton, C., A plate tectonic model of the eastern Indonesia collision zone, *Nature, 319*, 394-396, 1986.

De Boor, C., *A Practical Guide to Splines*, Springer-Verlag, New York, 1978.

DeMets, C., R.G. Gordon, D.F. Argus, and S. Stein, Current plate

motions, *Geophys. J. Int., 101*, 425-478, 1990.
DeMets, C., R.G. Gordon, D.F. Argus, and S. Stein, Effect of recent revisions of the geomagnetic reversal time scale on estimates of current plate motions, *Geophys. Res. Lett., 21*, 2191-2194, 1994.
Dow, D., and R. Sukamto, Western Irian Jaya: the end product of oblique plate convergence in the late Tertiary, *Tectonophysics, 106*, 109-139, 1984.
Dziewonski, A. M., T.-A. Chou, and J. H. Woodhouse, Determination of earthquake source parameters from waveform data for studies of global and regional seismicity, *J. Geophys. Res., 86*, 2825-2852, 1981.
Dziewonski, A. M., G. Ekström, and M. P. Salagnik, Centroid-moment tensor solutions for July-September 1995, *Phys. Earth Planet. Inter., 97*, 3-13, 1996.
Fitch, T. J., Plate convergence, transcurrent faults and internal deformation adjacent to southeast Asia and the western Pacific, *J. Geophys. Res., 77*, 4432-4460, 1972.
Fung, Y.C., *Foundations of Solid Mechanics*, Prentice-Hall, Englewood Cliffs, N.J., 1965.
Genrich, J.F., Y. Bock, R. McCaffrey, E. Calais, C. Stevens, and C. Subarya, Accretion of the southern Banda arc to the Australian plate margin determined by Global Positioning System measurements; *Tectonics, 15*, 288-295, 1996.
Gordon, R.G., and S. Stein, Global tectonics and space geodesy, *Science, 256*, 333-342, 1992.
Haines, A. J., Calculating velocity fields across plate boundaries from observed shear rates, *Geophys. J. R. Astron. Soc., 68*, 203-209, 1982.
Haines, A. J., and W.E. Holt, A procedure for obtaining the complete horizontal motions within zones of distributed deformation from the inversion of strain rate data, *J. Geophys. Res., 98*, 12,057-12,082, 1993.
Haines, A. J., J. A. Jackson, W. E. Holt, and D.C. Agnew, Representing distributed deformation by continuous velocity fields, *Sci. Rep. 98/5*, Inst. of Geol. and Nucl. Sci., Wellington, New Zealand, 1998.
Hamburger, M.W., R.K. Cardwell, and B.L. Isacks, Seismotectonics of the northern Philippine island arc, in *The Tectonic and Geologic Evolution of Southeast Asian Seas and Islands: Part 2, Geophys. Monogr. Ser.*, vol. 27, edited by D.E. Hayes, pp. 1-22, AGU, Washington, D.C., 1983.
Hamilton, W., Tectonics of the Indonesian region, *U.S. Geol. Surv. Prof. Pap., 1078*, 345 pp., 1979.
Hayes, D.E., and S.D. Lewis, A geophysical study of the Manila Trench, Luzon, Philippines, 1, Crustal structure, gravity and regional tectonic evolution, *J. Geophys. Res., 89*, 9171-9195, 1984.
Heki, K., Horizontal and vertical crustal movements from three-dimensional very long baseline interferometry kinematic reference frame: Implication for the reversal timescale revision, *J. Geophys. Res., 101*, 3187-3198, 1996.
Holt, W. E., and A. J. Haines, The kinematics of northern South Island, New Zealand, determined from geologic strain rates, *J. Geophys. Res., 100*, 17,991-18,010, 1995.
Johnston, C., and C. Bowin, Crustal reactions resulting from the mid Pliocene to recent continent-island arc collision in the Timor region, *BMR J. Aust. Geol. Geophys., 6*, 223-243, 1981.
Karig, D.E., A.J. Barber, T.R. Charlton, S. Klemperer, and D.M. Hussong, Nature and distribution of deformation across the Banda arc-Australia collision zone at Timor, *Geol. Soc. Am. Bull., 98*, 18-32, 1987.
Kato, T., et al., Initial results from WING, the continuous GPS network in the western Pacific area, *Geophys. Res. Lett., 25*, 369-372, 1998.
Kostrov, V.V., Seismic moment and energy of earthquakes, and seismic flow of rocks, *Izv. Acad. Sci. USSR Phys. Solid Earth*, Engl. Transl., *1*, 23-44, 1974.
Larson, K.M., J.T. Freymueller, and S. Philipsen, Global plate velocities from the Global Positioning System, *J. Geophys. Res., 102*, 9961-9981, 1997.
Love, A.E.H., *A Treatise on the Mathematical Theory of Elasticity*, Dover, Mineola, N.Y., 1944.
Lynnes, C. S., and T. Lay, Source process of the great 1977 Sumba earthquake, *J. Geophys. Res., 93*, 13,407-13,420, 1988.
Mao, A.L., C.G.A. Harrison, and T.H. Dixon, Noise in GPS coordinate time series, *J. Geophys. Res., 104*, 2797-2816, 1999.
McCaffrey, R., Lithospheric deformation with the Molucca sea arc-arc collision: Evidence from shallow and intermediate earthquake activity, *J. Geophys. Res., 87*, 3663-3678, 1982.
McCaffrey, R., Active tectonics of the eastern Sunda and Banda arcs, *J. Geophys. Res., 93*, 15,163-15,182, 1988.
McCaffrey, R., Seismological constraints and speculations on Banda arc tectonics, *Neth. J. Sea Res., 24*, 141-152, 1989.
McCaffrey, R., Slip partitioning at convergent plate boundaries, in *Tectonic Evolution of Southeast Asia*, edited by R. Hall and D.J. Blundell, *Geol. Soc., Spec. Publ., 106*, 3-18, 1996.
McCaffrey, R., Statistical significance of the seismic coupling coefficient, *Bull. Seismol. Soc. Am., 87*, 1069-1073, 1997.
Newcomb, K.R., and W.R. McCann, Seismic history and seismotectonics of the Sunda arc, *J. Geophys. Res., 92*, 421-439, 1987.
Okal, E., Seismotectonic setting of the February 17, 1996 Biak, Indonesia earthquake, *Eos Trans. AGU, 77*(17), Spring Meet. Suppl., S184, 1996.
Pacheco, J.F., and L.R. Sykes, Seismic moment catalog of large shallow earthquakes, 1900 to 1989, *Bull. Seismol. Soc. Am., 82*, 1306-1349, 1992.
Pacheco, J. F., L. R. Sykes, and C. Scholz, Nature of seismic coupling along simple plate boundaries of the subduction type, *J. Geophys. Res., 98*, 14,133-14,159, 1993.
Peterson, E. T., and T. Seno, Factors affecting seismic moment release rates in subduction zones, *J. Geophys. Res., 89*, 10,233-10,248, 1984.
Pollitz, F.F., and T.H. Dixon, GPS measurements across the northern Caribbean plate boundary zone: Impact of postseismic relaxation following historic earthquakes, *Geophys. Res. Lett., 25*, 2233-2236, 1998.
Puntodewo, S.S.O., et al., GPS measurements of crustal deformation within the Pacific-Australia plate boundary zone in Irian Jaya, Indonesia, *Tectonophysics, 237*, 141-153, 1994.
Puspito, N. T., and K. Shimazaki, Mantle structure and seismotectonics of the Sunda and Banda arcs, *Tectonophysics, 251*, 215-228, 1995.
Rangin, C., M. Pubellier, N. Chamot-Rooke, C. Vigny, X. Le Pichon, M. Aurelio, and R. Quebral, Estimation of subduction rates along the Philippines trenches from GPS results (GEODYSSEA PROJECT), *Eos Trans. AGU, 78*(46), Fall Meet. Suppl., F169, 1997.
Ren, J., W.E. Holt, and B. Shen-Tu, The anti clockwise rotation of southeast Asia, *Eos Trans. AGU, 78*(46), Fall Meet. Suppl, F650, 1997.
Rowlett, H., and J. Kelleher, Evolving seismic and tectonic patterns along the western margin of the Philippine Sea plate, *J. Geophys. Res., 81*, 3518-3524, 1976.
Scholz, C. H., and J. Campos, On the mechanism of seismic decoupling and back arc spreading at subduction zones, *J. Geophys. Res., 100*, 22,103-22,115, 1995.
Seno, T., and K. Kurita, Focal mechanisms and tectonics in the Taiwan-Philippine region, *J. Phys. Earth, 26*, S249-S263, 1978.
Seno, T., S. Stein, and A. E. Gripp, A model for the motion of the Philippine Sea plate consistent with NUVEL-1 and geological data, *J. Geophys. Res., 98*, 17,941-17,948, 1993.
Shen-Tu, B., W. E. Holt, and A. J. Haines, The contemporary kinematics of the western United States determined from earthquake moment tensors, very long baseline interferometry, and GPS observations, *J. Geophys. Res., 103*, 18,087-18,117, 1998.
Shen-Tu, B., W.E. Holt, and A.J. Haines, Deformation kinematics in the western United States determined from Quaternary fault slip rates and recent geodetic data, *J. Geophys. Res., 104*, 28,927-28,955, 1999.
Silver, E.A., R. McCaffrey, and R.B. Smith, Collision, rotation, and the initiation of subduction in the evolution of Sulawesi, Indonesia, *J. Geophys. Res., 88*, 9407-9418, 1983.
Simons, W.M.F., B.A.C. Ambrosius, R. Noomen, D. Angermann, P. Wilson, M. Becker, E. Reinhart, A. Walpersdorf, and C. Vigny, Observing plate motions in SE Asia: Geodetic results of the GEODYSSEA project, *Geophys. Res. Lett., 26*, 2081-2084, 1999.
Snyder, D.B. H. Prasetyo, D.J. Blundell, C.J. Pigram, A.J. Barber, A. Richardson, and S. Tjokosaproetro, A dual doubly vergent orogen in the Banda Arc continent-arc collision zone as observed on deep seismic reflection profiles, *Tectonics, 15*, 34-53, 1996.
Spence, W., The 1977 Sumba earthquake series: Evidence for slab pull force acting at a subduction zone, *J. Geophys. Res., 91*, 7225-7239, 1986.
Stein, S., Space geodesy and plate motions, in *Contributions of Space Geodesy to Geodynamics: Crustal Dynamics, Geodyn. Ser.*, vol. 23, edited by D.E. Smith and D.L. Turcotte, pp. 5-20, AGU, Washington, D.C., 1993.
Stevens, C., R. McCaffrey, Y. Bock, J. Genrich, Endang, C. Subarya, S.S.O. Puntodewo, Fauzi, and C. Vigny, Rapid rotations about a vertical axis in a collisional setting revealed by the Palu fault, Sulawesi, Indonesia, *Geophys. Res. Lett., 26*, 2677-2680, 1999.

Stewart, G.S., Implications for plate tectonics of the August 19, 1977 Indonesian decoupling normal fault earthquake, *J. Geophys. Res., 83*, 5041-5055, 1978.

Tinnon, M. J., W. E. Holt, and A. J. Haines, Velocity gradients in the northern Indian Ocean inferred from earthquake moment tensors and relative plate velocities, *J. Geophys. Res., 100*, 24,315-24,329, 1995.

Tregoning, P., et al., Estimation of current plate motions in Papua New Guinea from Global Positioning System observations, *J. Geophys. Res.*, 103, 12,181-12,203, 1998.

Walpersdorf, A., C. Vigny, C. Subarya, and P. Manurung, Monitoring of the Palu-Koro Fault (Sulawesi) by GPS, *Geophys. Res. Lett., 25*, 2313-2316, 1998.

Weissel, J. K., and R. N. Anderson, Is there a Caroline plate?, *Earth Planet. Sci. Lett., 41*, 143-158, 1978.

Wessel, P., and W.F. Smith, Free software helps map and display data, *Eos Trans. AGU, 72*, 441, 1991.

Yu, S.-B., L.-C. Kuo, R.S. Punongbayan, and E.G. Ramos, GPS observation of crustal deformation in the Taiwan-Luzon region, *Geophys. Res. Lett., 26*, 923-926, 1999.

S. Goes, Institut für Geophysik, ETH Hönggerberg, CH-8093, Zurich, Switzerland. (saskia@tomo.ig.crdw.cthz.ch)

R. Govers, Institute of Earth Sciences, Utrecht University, P. O. Box 80.021, 308 TA, Utrecht, Netherlands. (govers@geo.uu.nl)

W. E. Holt and C. Kreemer, Department of Geosciences, State University of New York at Stony Brook, Stony Brook, NY 11794-2100. (holt@horizon.ess.sunysb.edu; kreemer@horizon.ess.sunysb.edu)

(Received February 19, 1999; revised September 15, 1999; accepted September 30, 1999)